JOURNAL OF MATERIALS SCIENCE **38** (2003) 4745–4755

SiC-particulate aluminum composite foams produced by powder compacts: Foaming and compression behavior

S. ELBIR*, S. YILMAZ‡, A. K. TOKSOY§, M. GUDEN§,¶
*Materials Science and Engineering Program, Departments of ‡Chemical Engineering and §Mechanical Engineering, İzmir Institute of Technology, Izmir, Turkey
E-mail: mustafaguden@iyte.edu.tr

I. W. HALL
Department of Mechanical Engineering, University of Delaware, Newark, DE 19716, USA

The foaming behavior of SiC-particulate (8.6% by volume) aluminum composite powder compacts contained Titanium Hydride blowing agent was investigated by heating above the melting temperature (750°C) in a pre-heated furnace. Aluminum powder compacts were also prepared and foamed using similar compaction and foaming parameters in order to determine the effect of SiC-particulate addition on foaming and compression behavior. The linear expansions of the compacts at various furnace holding times were *ex situ* determined. Optical and scanning electron microscopy techniques were used to characterize prepared and deformed foams microstructures. The SiC-particulate addition was found to increase the linear expansion and reduce the extent of the liquid metal drainage and cell coarsening of the aluminum compacts. The composite foam samples also showed higher compressive stresses, but a more brittle behavior as compared with aluminum foams.

1. Introduction

Aluminum (Al) closed-cell foams are materials of increasing importance because they have good energy absorption capabilities combined with good thermal and acoustic properties. They can convert much of the impact energy into plastic energy and absorb more energy than bulk metals at relatively low stresses [1]. When used as filling materials in tubes, they increase total energy absorption over the sum of the energy absorbed by foam alone and tube alone [2, 3].

Al closed-cell foams are currently manufactured by several different processes. In a process patented by Alcan International Limited, the liquid metal is foamed by injecting gases (e.g., air or nitrogen) into the melt [4]. In the Alporas process, developed in Japan, a blowing agent (TiH_2) is added into the melt and the melt is then stirred quickly in order to form a homogeneous distribution of blowing agent [5]. The decomposition of the blowing agent, which releases hydrogen gas into the melt, drives the expansion of the melt. Foaming of powder compact process, patented by, e.g., Fraunhofer CMAM, starts with mixing and compaction of metal powders with a blowing agent in order to form a foamable precursor material [6]. Heating of the precursor to or above the melting temperature results in decomposition of blowing agent and simultaneously expansion of the precursor. In the Formgrip process, a passivated blowing agent is directly incorporated into the liquid metal, which is subsequently cast to obtain a foamable precursor [7]. The precursor is heated to an elevated temperature in order to drive the decomposition reaction of the blowing agent.

Due to their large surface area, liquid metal foams are unstable. Therefore, they are usually stabilized by adjusting liquid metal viscosity; either by adding fine ceramic particles or alloying elements into the melt. In the Alcan process, liquid foam is stabilized by adding 8–20 μm size SiC particles [8]. The foamable precursor in the Formgrip process is a SiC-particulate Metal Matrix Composite (SiC_p/MMC) [7]. The viscosity of the liquid metal in the Alporas process is adjusted by Ca-addition into the melt, resulting in formation of oxide particles by internal oxidation [5]. In the foaming of powder compact process, foam stabilization was ascribed to the metal oxide filaments which are remnants of the thin oxide layer on the aluminum powders and/or the solid component of the particular alloy (Al-rich phase in the Al-Si eutectic) [8, 9]. In a previous study, it was experimentally shown that lead powder higher in oxygen content exhibited a more stable foaming behavior than powder lower in oxygen content [8].

¶Author to whom all correspondence should be addressed.

TABLE I Specifications of raw materials. D is the particle size and (X%) is the percentage of the particles smaller than the given value

Powders	Size (μm)	Purity	Measured mean diameter (μm)	D (10%) (μm)	D (50%) (μm)	D (90%) (μm)
Al powder (Aldrich)	<74	99%	37.13	17.32	34.64	69.28
TiH_2 (Merck)	<37	>98%	–	–	–	–
SiC_p(Aldrich)	<37		20.12	12.25	22.36	33.4

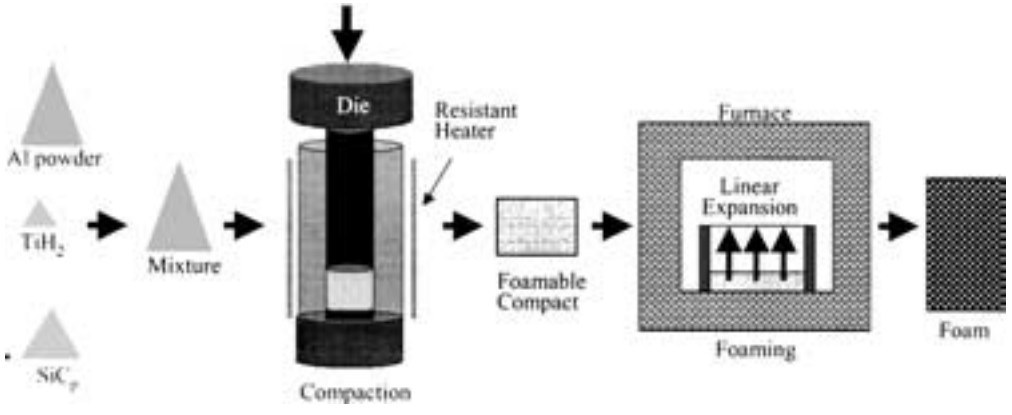

Figure 1 Schematic of foam preparation method.

This study aims at determining the effect of SiC_p on the foaming behavior of aluminum powder compacts, which, according to our knowledge, has not been investigated previously. For that purpose, SiC_p/Al MMC and Al powder compacts were prepared and foamed. The effect of SiC_p-addition on the foaming behavior was determined by comparing the actual linear expansions of the SiC_p/Al and Al compacts processed under the same conditions. Compression testing on the prepared composite and Al foams was conducted in order to determine the effect of SiC_p-addition on the crushing behavior.

2. Materials and experimental

The specifications of materials, aluminum powder, TiH_2 (blowing agent) and SiC_p used to prepare foams are listed in Table I. The particle sizes of the Al powder and SiC_p were measured with a Micromeritics Particle Size Analyzer. Mean particle sizes were found to be 37 and 22 μm for Al powder and SiC_p, respectively. Aluminum powder with a relatively low impurity content (>1%) was preferred over an alloy powder in order to reduce the extent of reactions between SiC_p and alloying elements. The main studies on foaming behavior were conducted on 8.6 volume percentage (10 wt%) SiC_p compacts although a few 20% SiC_p/Al composite foam samples were also prepared and compression tested. The content of blowing agent was chosen to be 0.5 wt%, an amount found to be sufficient for foaming of aluminum compacts [10].

The foam preparation method is schematically shown in Fig. 1. The process starts with the mixing of appropriate amounts of basic ingredients (Al powder, TiH_2 and SiC_p) inside a plastic container, which was rotated on a rotary mill in order to form a homogeneous powder mixture. Compacts with a diameter of 27 mm and a thickness of 9.5 mm were prepared from the powder mixture inside a stainless steel die, see Fig. 1. Compaction was initially conducted at room temperature for a few minutes and followed by hot compaction for 30 min. A resistance heater placed around the die was used to heat the die to the hot compaction temperature (Fig. 1). The heating cycle, from room temperature to compaction temperature, was one hour. During cold and hot compactions and heating cycle the die pressure was kept constant at 220 MPa.

Foaming experiments were conducted in a pre-heated furnace at a temperature of 750°C, higher than the melting temperature of Al. The cold compacts were inserted into the furnace inside a steel tube having the same diameter as the compact and a length of 8 cm. The steel tube was tightly closed at the bottom and placed vertically into the furnace so that expansion was limited to only the vertical direction as designated with arrows in Fig. 1. Inserting and removing specimen took less than 10 s. For each experiment furnace temperature was recorded and found to vary plus or minus 10°C during foaming. Initial experiments were aimed

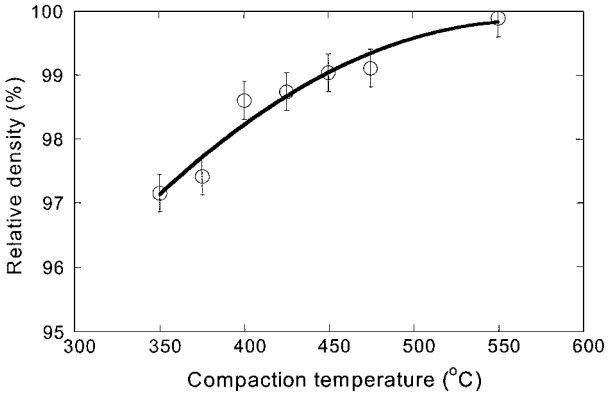

Figure 2 Relative density (%) as a function of compaction temperature of Al compacts.

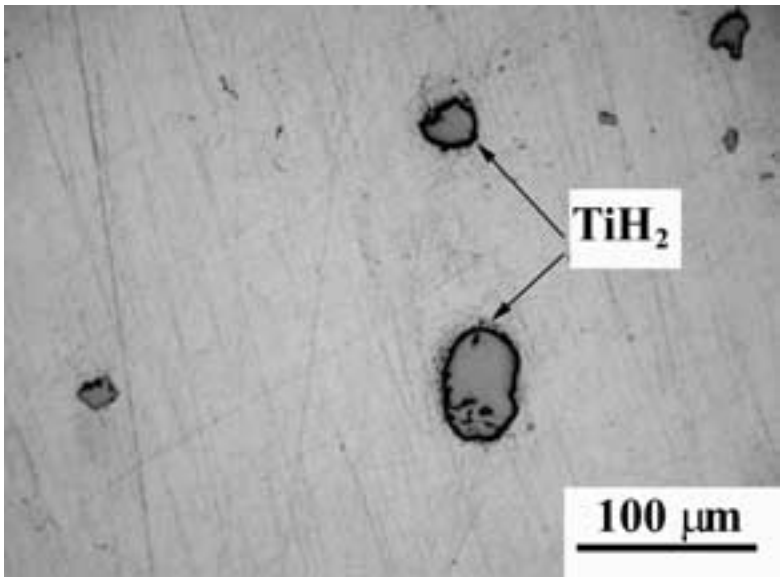

(a)

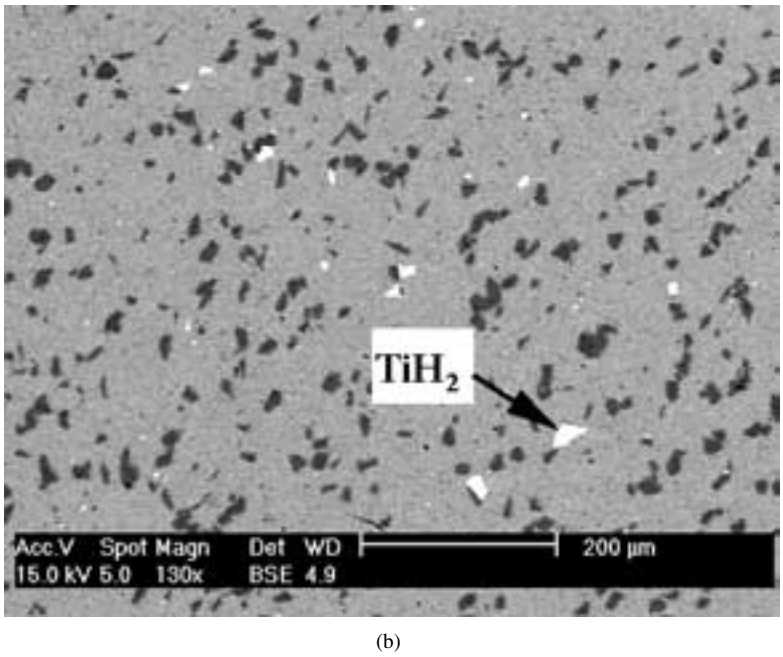

(b)

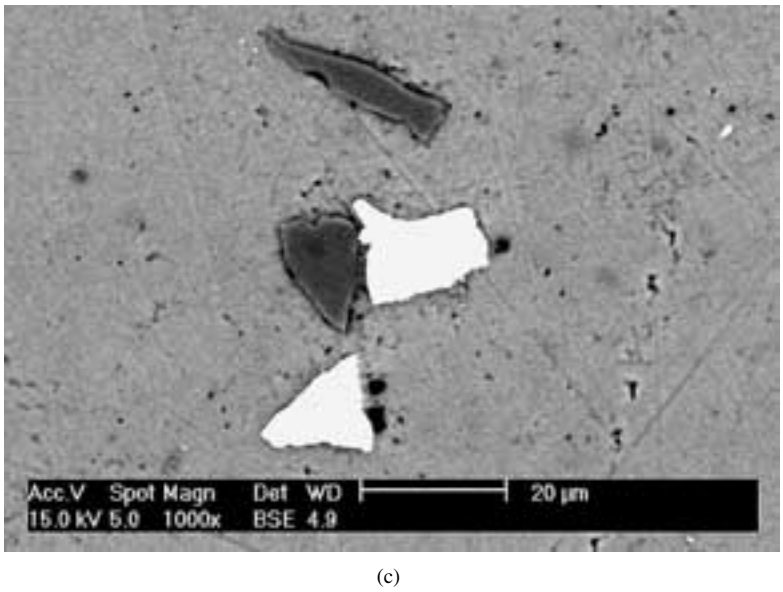

(c)

Figure 3 Optical and BSE micrographs of: (a) Al, (b) and (c) 8.6% SiC_p/Al compacts.

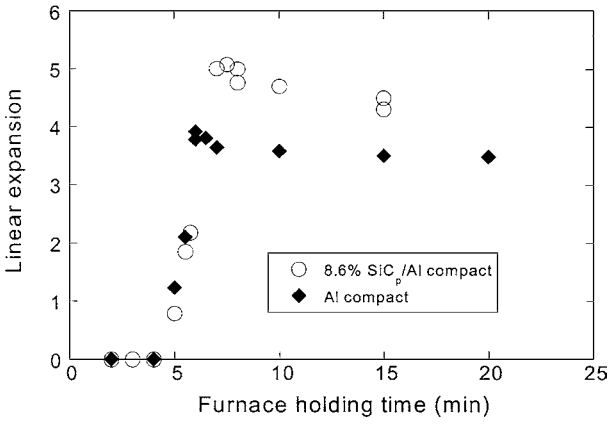

Figure 4 LEs vs. furnace holding time of SiC_p/Al and Al compacts.

at determining the effect of furnace holding time on the linear expansion of the compacts. Therefore, foamed or partially foamed compacts were taken from the furnace after a specified furnace-holding time. These samples were quickly cooled on a large steel plate by spraying water onto the steel tube. Foam sample heights were measured in order to calculate linear expansion and then were sectioned longitudinally with a diamond saw for microscopic observations. Microstructural examinations were performed using optical microscopy and a Philips XL30-SFEG scanning electron microscope in both Secondary Electron (SE) and Back-Scattered Electron (BSE) modes. Compositional analysis was conducted using an Energy Dispersive X-ray (EDX) analyzer.

A second group of foams were prepared for the mechanical testing using the same process outlined above. In order to prepare foams of different densities, samples were taken from the furnace after various holding times. From these samples, cylindrical test specimens, 20 mm in height and 20 mm in diameter, were core-drilled. During core-drilling the pressure was kept as low as possible in order not to induce plastic deformation in the foam specimens. Compression tests were conducted using an Instron testing apparatus at a cross-head speed of 0.1 mm s^{-1}.

3. Results and discussions

Previous study on Al powder compaction for foamable compacts has shown that maximum expansion was attained with hot-compaction temperatures between 400 and 450°C [10]. At lower compaction temperatures, the hydrogen escaped through the interconnected porosity without expanding the compact during heating in the furnace and the minimum relative density for an efficient foaming was given as 99% [10]. The compaction temperatures above 500°C were also found to be enough to drive all the hydrogen from the compact in the compaction stage [10]. The effect of compaction temperature on the relative density of the Al compacts (220 MPa and 30 min hot compaction) is shown in Fig. 2 and the compact densities around 99% or higher were only achieved at compaction temperatures higher than 425°C. Since higher temperatures will increase TiH_2 decomposition, 425°C was chosen as the compaction temperature for the studied Al and SiC_p/Al composite powder compacts. Fig. 3a and b are the microstructures of the prepared Al and composite powder compacts, respectively. Al and composite compacts had relatively homogenous distributions of the particles (SiC and TiH_2) and macroscopically contained no porosity as depicted in Fig. 3c.

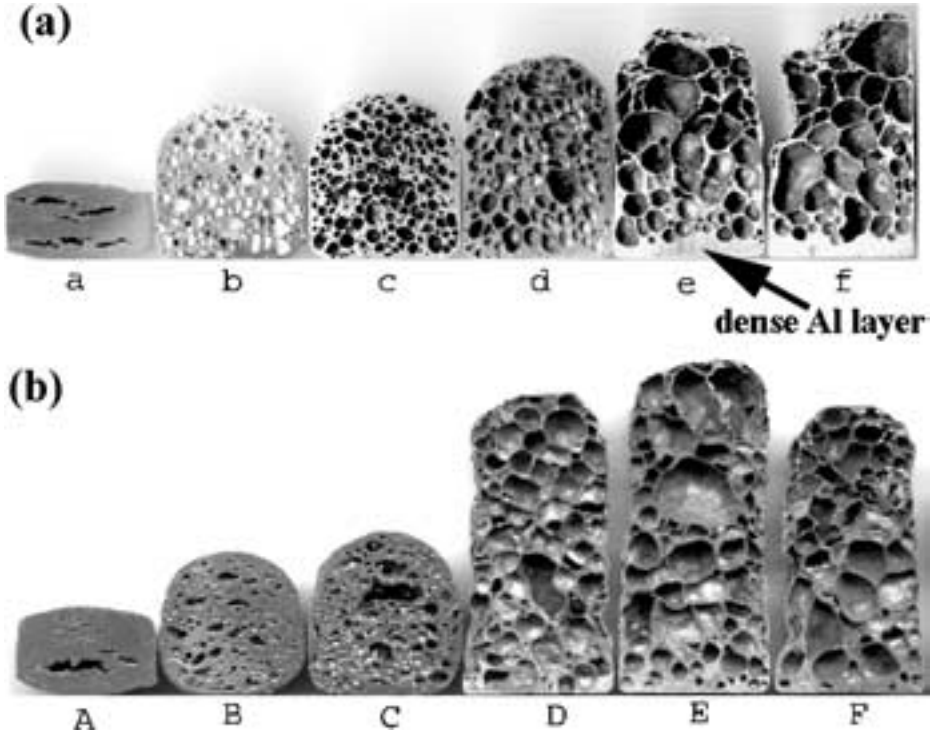

Figure 5 Foam structure evolution as a function of furnace holding time: (a) Al compacts; a = 5, b = 5.30, c = 5.45, d = 6, e = 10 and f = 15 and (b) 8.6% SiC_p/Al compacts; A = 5, B = 5.45, C = 6, D = 7, E = 8 and F = 10 min.

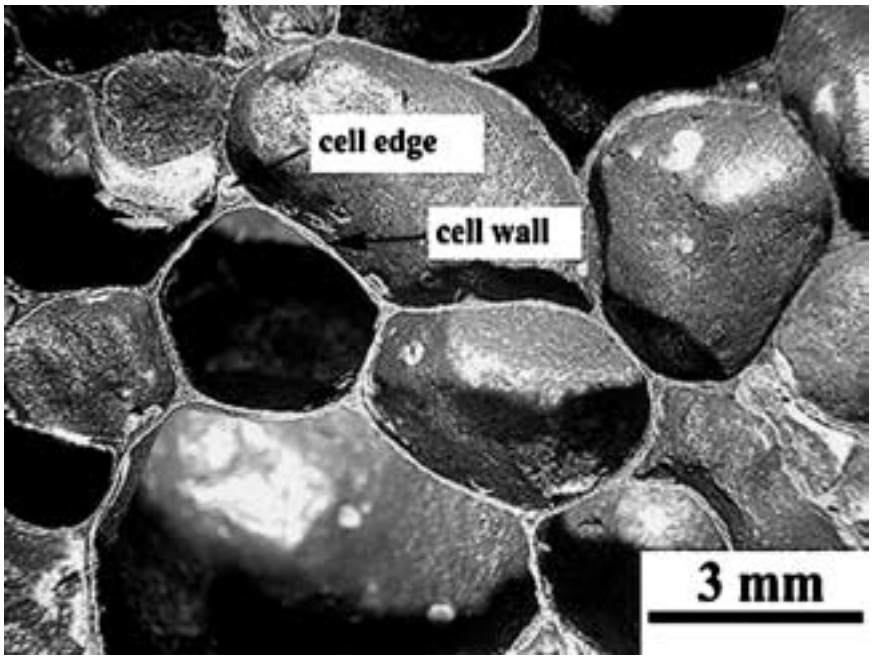

Figure 6 Optical micrograph of SiC_p/Al composite foam cell structure (LE = 5.2).

The linear expansions (LEs) of the composite and Al compacts are shown in Fig. 4 as a function of the furnace holding time. The LE was calculated using,

$$\mathrm{LE} = \frac{h_\mathrm{f} - h_\mathrm{o}}{h_\mathrm{o}} \tag{1}$$

where h_f and h_o are the height of the foam measured after a specific furnace holding time and initial height of the foamed compact, respectively. For both compacts foaming started about 5 min (Fig. 4). During this time, the compact was presumably being heated to some critical temperature before foaming started. It is also noted that LEs of the composite and Al compacts increased rapidly to a maximum and then decreased slightly with increasing furnace holding time.

The foaming process unavoidably continues during cooling of the liquid foam after being taken from the furnace at a specific holding time. Therefore, the *ex situ* measured LEs (actual LEs) shown in Fig. 4 are expected to be different from the *in situ* measured LEs (real-time LEs). Previous *in situ* and *ex situ* LE measurements of foaming Al melts and compacts have shown that liquid foams being solidified in the region where the expansion increases almost linearly with holding time, had higher actual expansions, and vice versa if the foams were solidified in the region where the expansion remains almost constant or decreases slightly with increasing holding time [10, 11]. The difference between two was found to be 10% in terms of porosity, corresponding to a LE of 0.1 for the studied compacts [11]. This is negligible compared to measured LE values (4–5) in this study.

Previous studies on TiH_2 have shown a decomposition process starting at 380°C and ending at 570°C [10, 12]. The present hot compaction temperature was actually greater than the decomposition starting temperature of TiH_2; therefore, it is expected that some H_2 release would occur in the compaction, before foaming in the furnace. This excess H_2 was claimed to be loosely bound and released at early stage of the foaming, leading to a quick inflation of pores [10]. Since the LEs of the studied compacts were measured *ex situ*, the effect of excess hydrogen could not be determined.

Although foaming characteristics of the individual compacts prepared by the same processing routes may alter depending on several factors, such as spatial distribution of blowing agent in each compact and so on, some generalization could be made on the foaming sequence of the studied powder compacts based on Fig. 5a and b. These are: (i) at the early stage of expansion pores were elongated normal to the compaction direction, a, A, B and C, (ii) initially elongated pores became more spherical in the later stages as the porosity increased, b and c, and (iii) spherical pores were then deformed into polyhedral shape, d, e, D and E. It is also noted a thick metal layer Fig. 5a(e) formed at the bottom of Al foams and the vaulted shape disappeared at later stages of the foaming Fig. 5a(f). SiC_p/Al foams however maintained more regular cell shape. The actual LE values of the studied compacts can be further compared with the real-time LE of similar Al compacts. For example, the maximum real-time LEs for 6061 Al and Al-Si (Si particles were added in the powder processing stage) alloy compacts at 800°C were found to be 3 and 4–5, respectively [10]. Somewhat similar maximum LEs were measured in this study; approximately 4 and 5 for Al and 8.6% SiC_p/Al compacts respectively.

The foaming process may be considered in 3 stages: pore formation, growth and collapse [13]. Above the decomposition temperature of the blowing agent, the evolving hydrogen gas accumulates in tiny voids of the precursor material. As the temperature increases to or near to the melting point of the precursor, pore growth occurs by the evolving gas. At latter stages, foam collapses via coarsening and drainage. Coarsening is due to the growth of the larger bubbles at

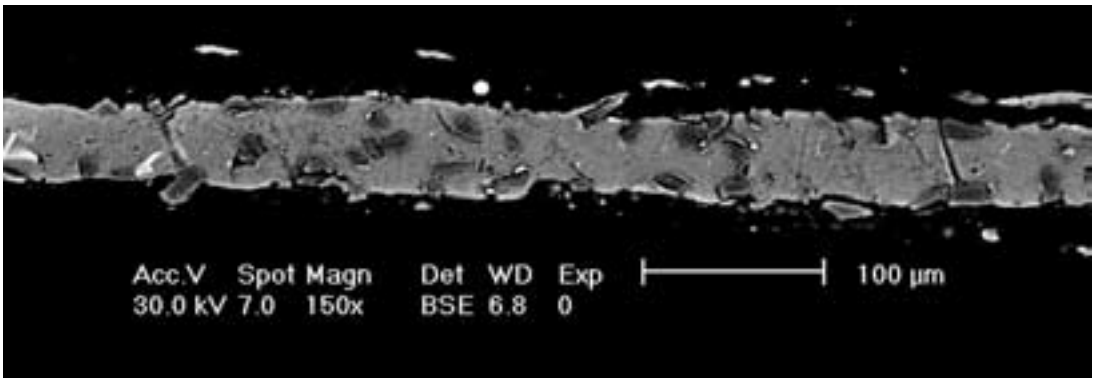

(a)

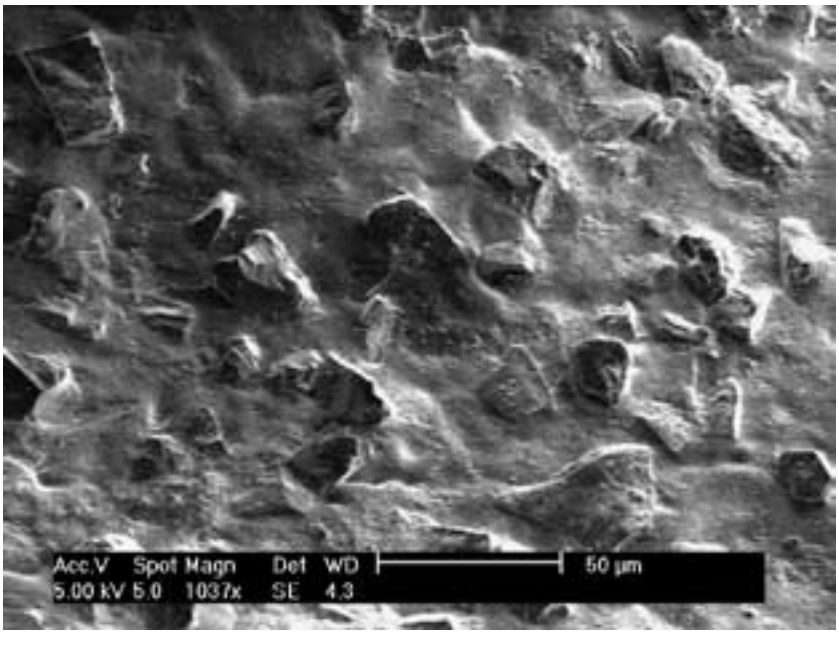

(b)

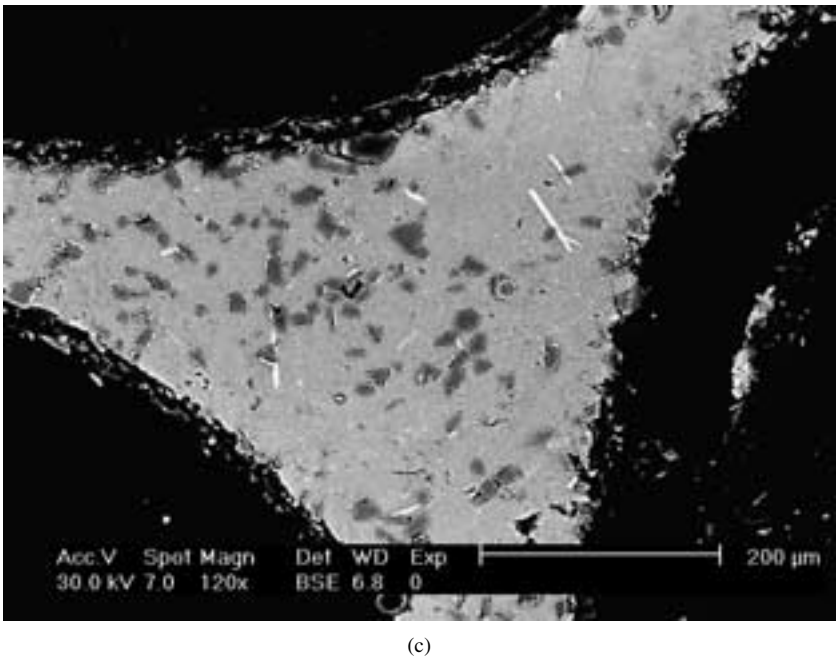

(c)

Figure 7 BSE and SE micrographs of 8.6% SiC_p/Al composite foam: (a) cell wall, (b) cell wall surface and (c) cell edge.

the expense of smaller ones. This may be driven by pressure differences between two adjacent bubbles or simply due to rupture of the cell wall of two adjacent bubbles. Drainage is the downward flow of the liquid metal through the cell edges due to gravitational forces. Drainage results in formation of thick dense layer of liquid metal at the bottom and cells with thicker walls in the middle.

The foaming sequence of the studied SiC_p/Al and Al compacts follow the above-mentioned stages. SiC_p/Al compacts, however, showed a reduced rate of coarsening and drainage as compared with Al compacts (Fig. 5a and b). As is explained previously, the presence of solid particles plays a critical role in liquid foam stabilization. Solid particles can increase melt bulk viscosity and they can also significantly contribute to increasing surface viscosity of the cell faces if a significant fraction of particles is located at the gas/melt interface. Both are effective in slowing down capillarity-driven melt flow from cell faces through cell edges (cell thinning) and gravity driven melt flow through cell edges (drainage) [7]. The solid particles may also have a destabilizing effect if an unsuitable particle size is selected for viscosity enhancement, especially when the size of the particles is in the range of cell face thickness [14]. The higher solid content of the foamed composite compacts is believed to be responsible for the enhanced foaming behavior. Besides SiC particles, the solid phases (e.g., Al_4C_3) forming as a result of reactions between SiC particles and Al melt may also contribute to enhancement of viscosity of foaming Al melt. Moreover, the milling of the Al powder together with SiC_p likely results in detachment of the oxide skin and consequently the retention of relatively small oxide particles. The thickness of oxide skin is believed to be in the range of 10 nms and cannot be resolved in the scanning electron microscope [9].

The cell structure of the prepared foams represents characteristic features of the conventional Al foams; thicker cell edges, curved and missing cell walls and

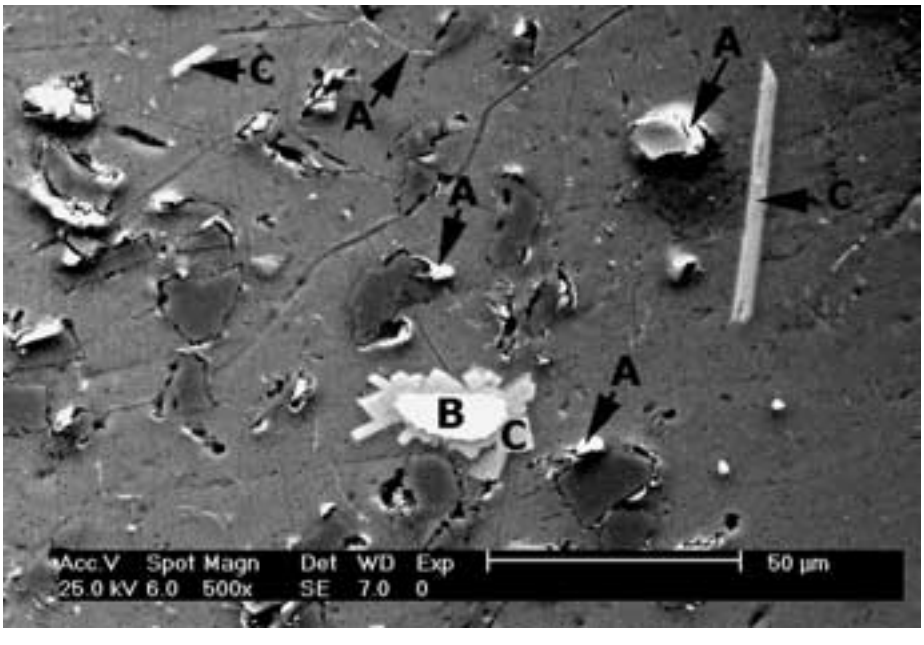

Figure 8 SE micrographs of SiC_p/Al composite foam cell edge, A:Al-Si-Fe, B:TiH_2 and C:Al-Ti.

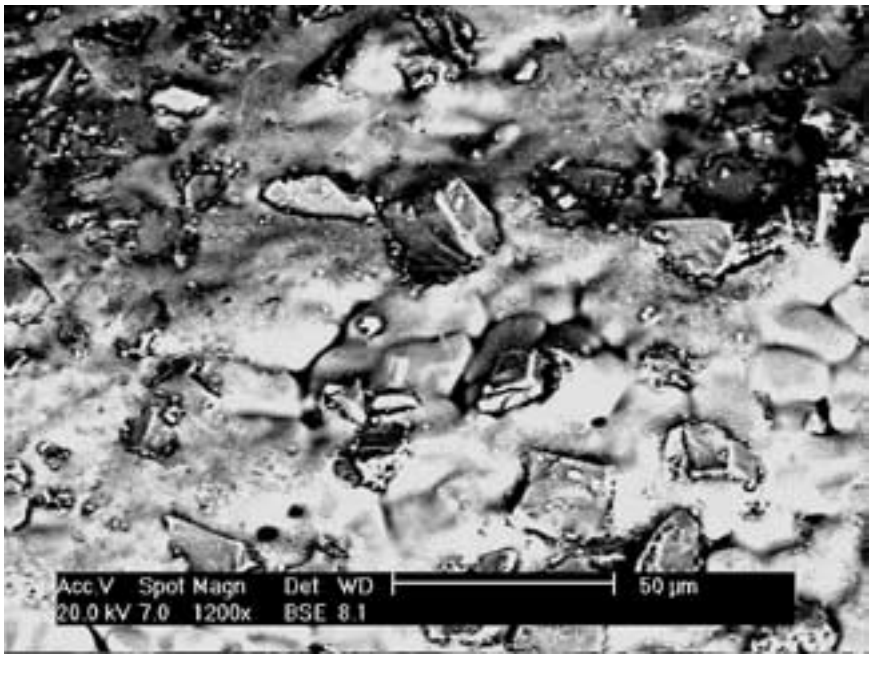

Figure 9 BSE micrograph of 8.6% SiC_p/Al composite foam cell surface, showing retained boundaries of the original particles.

nodes on the cell edges (Fig. 6). The SiC_p distribution across the cell wall, at the cell wall surface and in the cell edge of the 8.6% SiC_p/Al composite foam is shown sequentially in Fig. 7a, b and c. Although, particles are preferentially located at cell wall surface/gas interface, similar to the SiC_p/Al foams produced by Alcan [15] and Formgrip processes [7], a significant fraction of the particles is also found in the interior of the cell wall and in the cell edge (Fig. 7a and c), proving the potential of the SiC_p for the enhancement of the bulk and surface viscosities.

It is known that SiC reacts with molten Al, producing brittle Al_3C_4 and Si-rich Al phases. Microscopic studies on SiC_p/Al composites have shown Al_4C_3 formed around the SiC particles, seen as the dark patches at the interfaces and surfaces of the particles under the microscope and Si simultaneously diffused through the melt, forming an Si-rich band around SiC particles [16, 17]. Similarly, a Si-rich region (8–13 wt%) around the SiC particles (A in Fig. 8) was detected using EDX analysis. It is also noted that a particularly large TiH_2 particle was only partially decomposed (B in Fig. 8) and formed an Al-Ti compound (C in Fig. 8).

One of the features of the prepared SiC_p composite and Al foams is that the original particle boundaries were retained on the cell walls (Figs 9 and 10). Particle boundaries were also observed in 6061 Al and Al-Si foams produced by the foaming from powder compacts method [10, 18]. During foaming, the unmelted oxide skin on the Al powder most likely results in retention

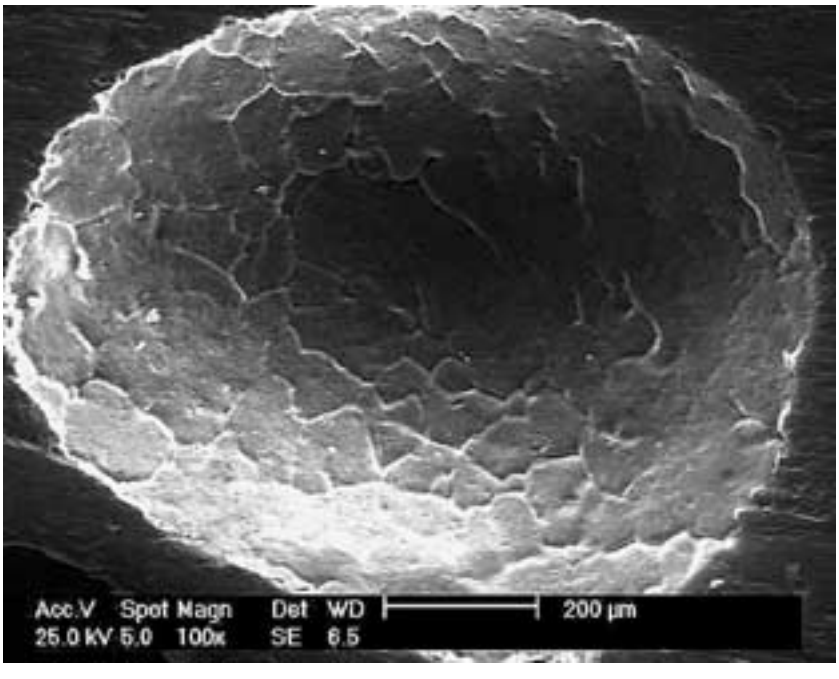

Figure 10 SE micrograph of the interior of a cell of Al foam, showing retained boundaries of the original particles on the cell wall surface.

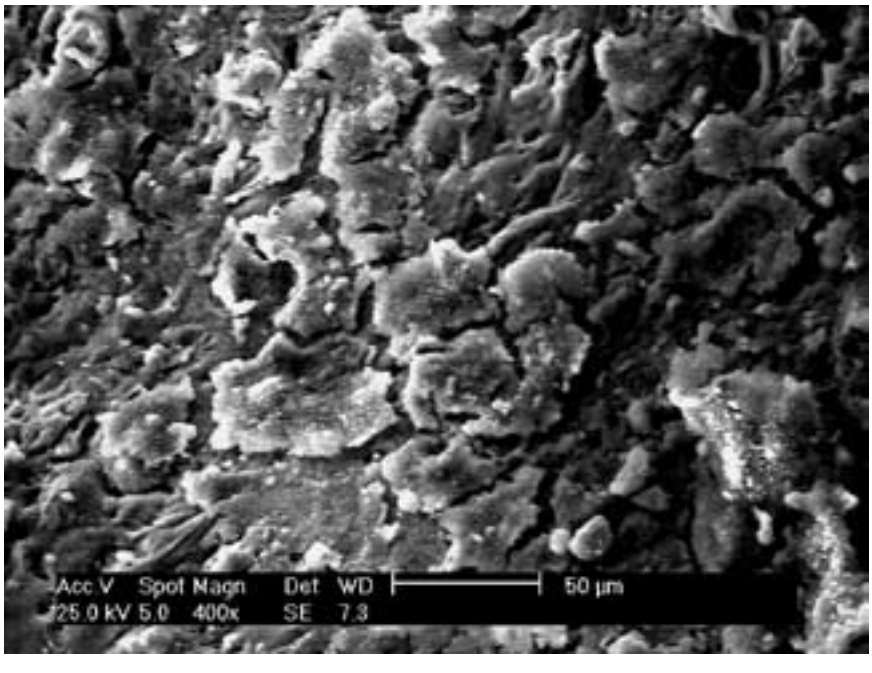

Figure 11 SE micrograph of the cell wall surface of the Al foam, showing fractured oxide rich-skin.

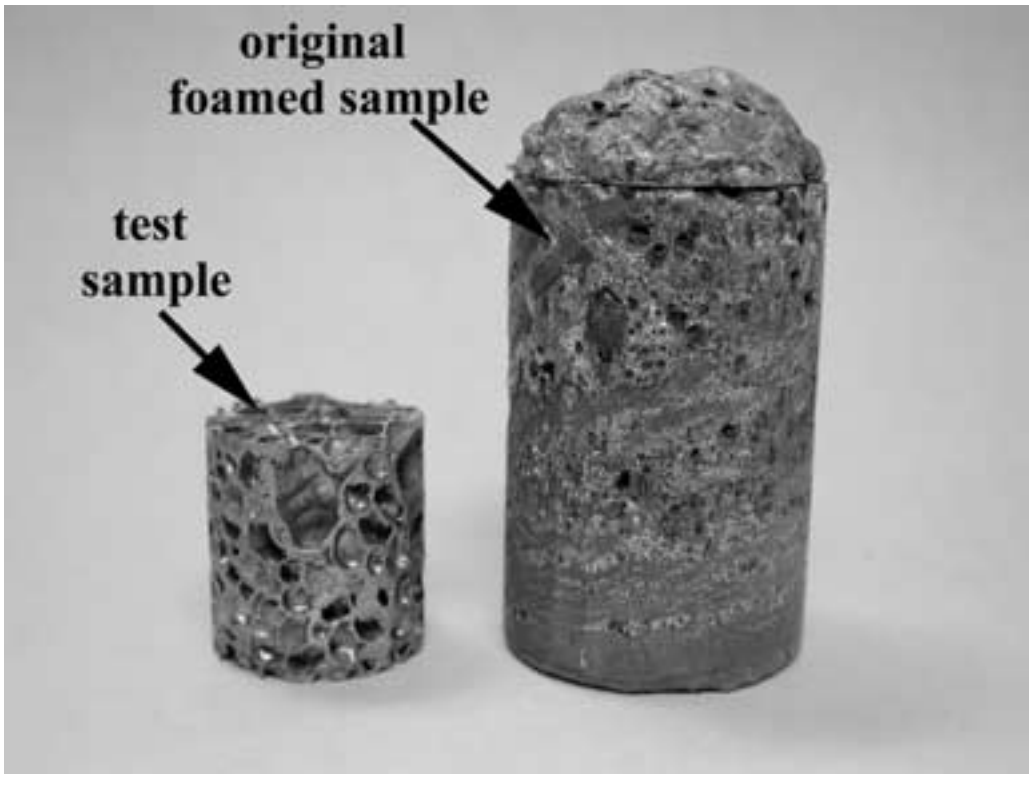

Figure 12 Cylindrical compression test sample (left) and the original foam specimen from which the test sample was core-drilled (right).

of the boundaries of the individual powders. An oxide-rich layer of metal on the surfaces of the cell wall of the Al foam was observed (Fig. 11). This layer is produced most likely by the reaction between molten Al and oxygen in the furnace. The cracks on the layer are due to differences in the thermal expansion coefficients of the oxide layer and underlying metal.

Typical compression test samples prepared by core drilling of the foamed sample, together with original foamed sample, are shown in Fig. 12. Fig. 13a and b show the effect of foam density on the compressive stress-strain behavior of the prepared Al and 8.6% SiC_p/Al foam samples, respectively. As shown in Fig. 14, the stress values and plateau stress of the SiC_p/Al foam are higher than those of Al foam at the same density. The difference in stress values decreases, however, as the deformation proceeds at large levels of strains.

Closed-cell Al foam has a characteristic compression stress-strain curve. It consists of three distinct regions: linear elastic, collapse and densification. In the linear elastic region, deformation is controlled by cell wall bending and/or stretching [1]. This region is followed by a collapse region which proceeds by spreading of deformation from localized to undeformed regions of the sample. This region is characterized by a stress plateau either with a constant value or increasing slightly with strain. At larger strains, cell walls start to touch each other and as a result of this, the material densifies. This deformation mechanism was also observed in the studied composite and pure Al foams.

Mechanical behavior of metallic foams has been reviewed recently by Gibson and it was shown that most of the commercially available closed-cell metallic foams behave as if their cells were open [19]. This is because surface tension draws much material to the cell edges and, therefore, during compression, thinner cell faces buckle and cell edges crush over the cell walls. Fig. 15 shows the typical deformed cell structure of

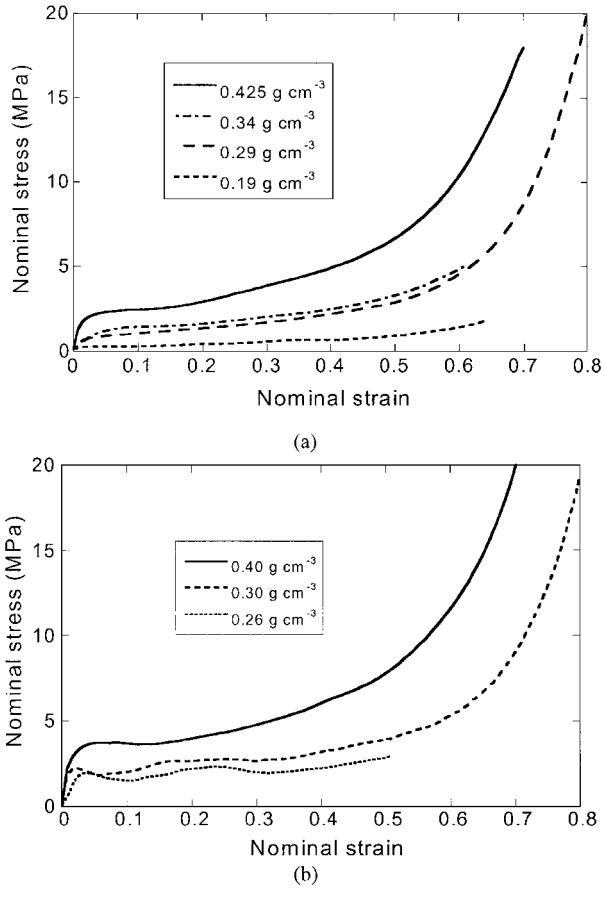

Figure 13 Compression stress-strain curves of: (a) Al and (b) 8.6% SiC_p composite foams at various densities.

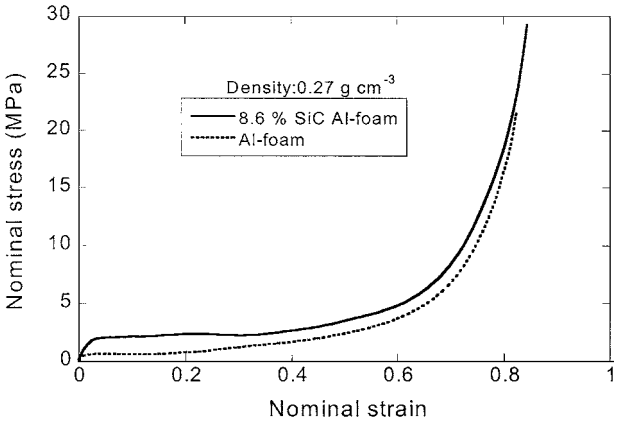

Figure 14 Compression stress-strain curves of Al and 8.6% SiC_p composite at the same density.

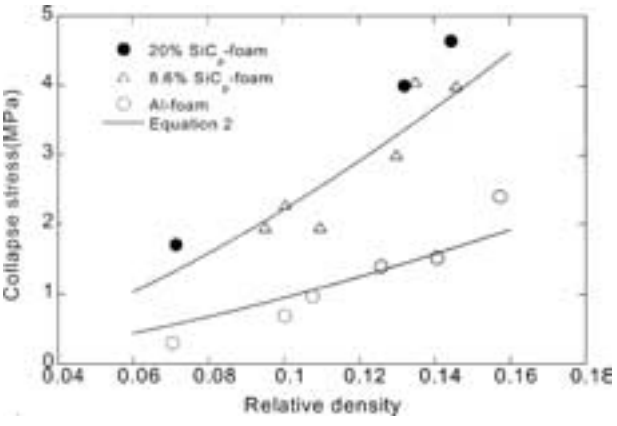

Figure 16 Variation of collapse stress with relative density.

the composite foam recovered after compression testing until 50% strain. Cell wall rupture and buckling are the main deformation mechanisms for the prepared Al and composite foams, although microscopically composite foams were found to contain more fractured cell wall sides as compared with the Al foams tested until the same final strain. The collapse stress or plateau stress of closed-cell foams can be fitted to the equation, which was developed for the open cell foams and given as [1].

$$\sigma_p = \sigma_y C(\rho^*)^{3/2} \quad (2)$$

where σ_p is the plateau stress, σ_y is the yield stress of the foaming metal, C is a constant related to cell geometry and ρ^* is the relative density of the foam (ratio of foam density to foaming metal density). Data for a wide range of foams suggested that $C \sim 0.3$ [19].

Equation 2 was fitted to the collapse stress (the initial plateau stress was taken as collapse stress) and results are shown in Fig. 16 as collapse stress vs. relative density. Density of the composite was calculated using the rule of mixtures (2.7 g cm^{-3} for Al and 3.23 g cm^{-3} for SiC_p). Fitting of experimental collapse stress data resulted in σ_y values of 230 and 90 MPa for composite and Al-foam, respectively.

It is also noted in Fig. 16 that increasing volume content of the SiC is not significantly effective in increasing collapse stress of the composite foams, which was previously observed in composite foams produced by Alcan process [15]. This shows that compression behavior of the composite foam is primarily determined by the cellular structure rather than the content of the SiC particles. It should also be noted that the comparison of compression behavior of the composite and Al foams is made on the samples having the same relative density. But, the cell morphology including cell wall and edge

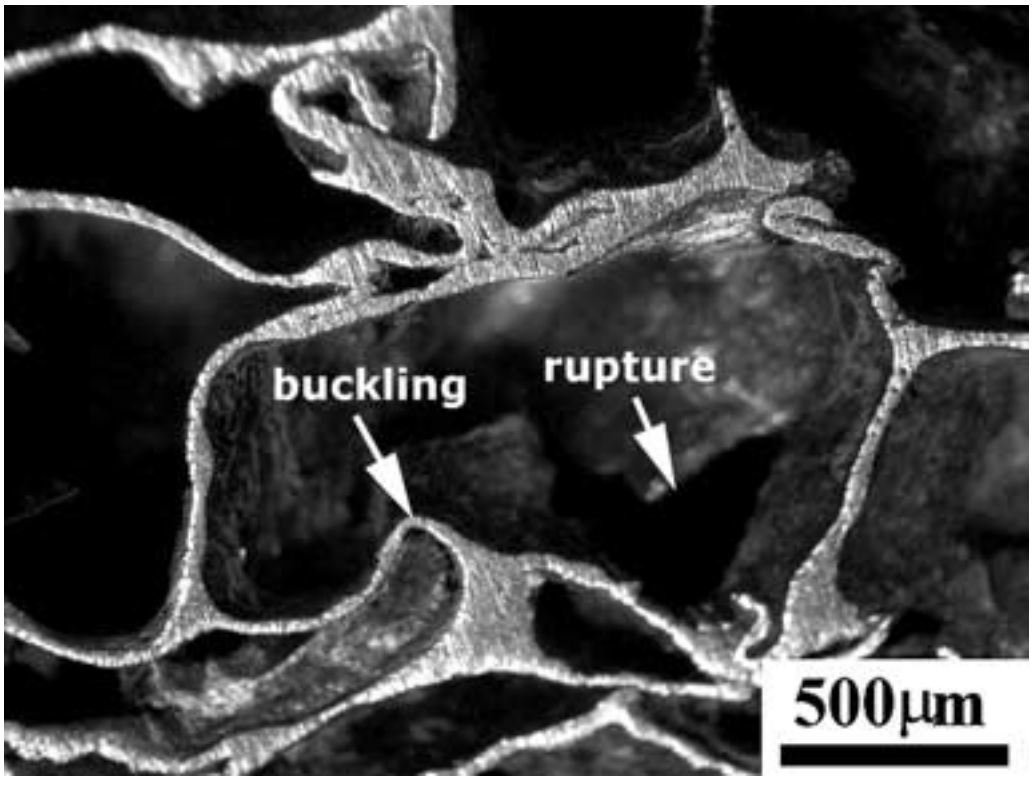

Figure 15 Optical micrograph of 8.6% SiC_p/Al foam (0.40 g cm^{-3}) compressed to 50% strain, showing cell wall rupture and buckling.

thickness was shown to affect the deformation behavior of Al foams greatly [20]. The cell morphology and its effects on the mechanical response of the prepared foams will be investigated in another study.

4. Conclusions

The effect of SiC-particles on the foaming behavior of Al powder compacts and on the compression behavior of the Al foams was investigated. It was found that SiC-particulate addition (a) increased linear expansion and (b) reduced the drainage and cell coarsening rates in Al compacts. The modified foaming behavior of the composite compact was attributed to higher solid particle content of the composite compact. SiC-particles also increased the foam compressive strength but induced a more brittle compression behavior. The microscopic analysis of the composite foams confirmed the presence several phases resulting from the reactions between SiC particles, TiH_2 powder and liquid Al in the foaming stage.

Acknowledgement

The authors would like to thank the Scientific and Technical Council of Turkey (TUBITAK) for the grant #MISAG-135.

References

1. L. J. GIBSON and M. F. ASHBY, "Cellular Solids: Structure and Properties" (Cambridge University Press, Cambridge, 1997) p. 309.
2. M. SEITZBERGER, F. G. RAMMERSTORFER, H. P. DEGISCHER and R. GRADINGER, *Acta Mech.* **125** (1997) 93.
3. A. G. HANSSEN, M. LANGSETH and O. S. HOPPERSTAD, *Int. J. Solids and Struct.* **24** (2000) 475.
4. I. JIN, D. L. KENNY and H. SANG, US Patent no. 4973358 (1990).
5. T. MIYOSHI, M. ITOH, S. AKIYAMA and A. KITAHARA, *Adv. Eng. Mater.* **2** (2002) 179.
6. J. BAUMEISTER and H. SCHRADER, US Patent no. 5151246 (1992).
7. V. GERGELY and B. CLYNE, *Adv. Eng. Mater.* **2** (2002) 175.
8. J. BANHART, *J. Metals* **12** (2000) 22.
9. *Idem.*, *Appl. Phys. Let.* **78** (2001) 1.
10. I. DUARTE and J. BANHART, *Acta Mater.* **48** (2000) 2349.
11. Z. SONG, J. ZHU, L. MA and D. HE, *Mater. Sci. Engnr.* **A298** (2001) 137.
12. F. BAUMGARTNER, I. DUARTE and J. BANHART, *Adv. Eng. Mater.* **2** (2000) 168.
13. J. BANHART, *Europhys. News* **30** (1999) 17.
14. V. GERGELY, R. L. JONES and B. CLYNE, High Temperature Capilarity (HTC-200), 19–22 November, 2000, Kurashiki, Japan.
15. L. D. KENEDY, *Mater. Sci. Forum* **217–222** (1996) 1883.
16. F. TONGXIANG, S. ZHONGLIANG, Z. DI and W. RENJIE, *Mater. Sci. Engnr.* **A257** (1998) 281.
17. T. SRITHARAN, L. S. CHAN, L. K. TAN and N. P. HUNG, *Mater. Character.* **47** (2001) 75.
18. I. W. HALL, M. GUDEN and C.-J. YU, *Scripta. Mater.* **43** (2000) 515.
19. L. J. GIBSON, *Annu. Rev. Mater. Sci.* **30** (2000) 191.
20. T. MIYOSHI, M. ITOH, T. MUKAI, H. KANAHASHI, H. KOHZU, S. TANABE and K. HIGASHI, *Scripta Mater.* **41** (1999) 1055.

Received 13 November 2002
and accepted 9 July 2003